Original Article

Modeling of solar UV-induced photodamage on the hair follicles in human skin organoids

Journal of Tissue Engineering
Volume 15: 1–20

DOI: 10.1177/20417314241248753
journals.sagepub.com/home/tej
Sage

Min-Ji Kim[1], Hee-Jin Ahn[2], Dasom Kong[1], Seunghee Lee[3], Da-Hyun Kim[1,4] and Kyung-Sun Kang[1]

Abstract

Solar ultraviolet (sUV) exposure is known to cause skin damage. However, the pathological mechanisms of sUV on hair follicles have not been extensively explored. Here, we established a model of sUV-exposed skin and its appendages using human induced pluripotent stem cell-derived skin organoids with planar morphology containing hair follicles. Our model closely recapitulated several symptoms of photodamage, including skin barrier disruption, extracellular matrix degradation, and inflammatory response. Specifically, sUV induced structural damage and catagenic transition in hair follicles. As a potential therapeutic agent for hair follicles, we applied exosomes isolated from human umbilical cord blood-derived mesenchymal stem cells to sUV-exposed organoids. As a result, exosomes effectively alleviated inflammatory responses by inhibiting NF-κB activation, thereby suppressing structural damage and promoting hair follicle regeneration. Ultimately, our model provided a valuable platform to mimic skin diseases, particularly those involving hair follicles, and to evaluate the efficacy and underlying mechanisms of potential therapeutics.

Keywords

Skin organoids, hair follicles, photodamage, NF-κB pathway, exosome

Date received: 6 December 2023; accepted: 6 April 2024

Graphic abstract

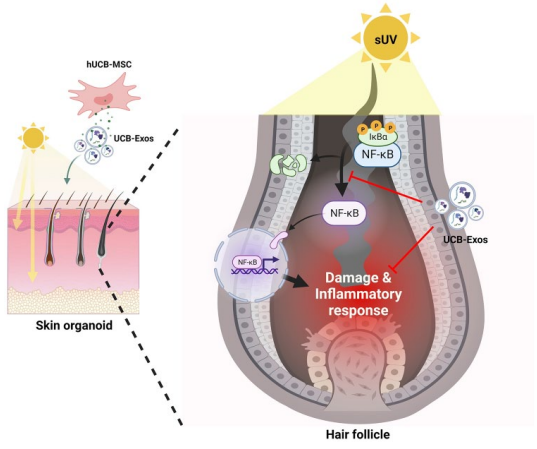

[1]Adult Stem Cell Research Center and Research Institute for Veterinary Science, College of Veterinary Medicine, Seoul National University, Seoul, Republic of Korea
[2]Cytotherapy R&D Center, PRIMORIS THERAPEUTICS CO., LTD., Gwangmyeong-si, Gyeonggi-do, Republic of Korea
[3]Stem Cell and Regenerative Bioengineering Institute, Global R&D Center, Kangstem Biotech Co., Ltd., Geumcheon-gu, Seoul, Republic of Korea
[4]Department of Biotechnology, Sungshin Women's University, Seoul, Republic of Korea

Corresponding authors:
Kyung-Sun Kang, Adult Stem Cell Research Center and Research Institute for Veterinary Science, College of Veterinary Medicine, Seoul National University, 1 Gwanak-ro, Seoul 08826, Republic of Korea.
Email: kangpub@snu.ac.kr

Da-Hyun Kim, Adult Stem Cell Research Center and Research Institute for Veterinary Science, College of Veterinary Medicine, Seoul National University, 1 Gwanak-ro, Seoul 08826, Republic of Korea., Department of Biotechnology, Sungshin Women's University, Seoul 01133, Republic of Korea.
Email: dahyun0515@snu.ac.kr

Introduction

The skin, which is the outermost layer of the body, performs crucial roles in protecting the body from potential harm in the external environment. However, excessive and prolonged exposure to solar ultraviolet (sUV) radiation has detrimental effects on skin functions. The cutaneous reactions after sUV radiation primarily accompany symptoms like rashes, wrinkling, skin sagging, and it can further progress to photoaging, actinic keratosis, or skin cancer.[1] Moreover, sUV radiation can also affect hair follicles as well as hair shafts, leading to hair loss, aging, and hyperpigmentation.[2,3] Due to the increasing incidence of UV-induced skin diseases, they have been a significant global health concern.[4] Therefore, numerous therapeutic interventions besides medications have been developed to alleviate photodamage by using in vitro skin models.[5,6] So far, research and development of therapeutics for skin diseases have been mainly conducted by using animal models.[7] However, there are discrepancies in anatomical compositions and physiology between human and animal skin, animal studies may not accurately predict results seen in humans.[8] Since the European Union banned the use of animals in cosmetic testing in 2013, the need to develop physiologically similar skin models and three-dimensional human skin models has rapidly increased.[8] In this regard, numerous attempts have been made to fabricate the skin substitutes or skin models *in vitro*, such as stacking 2D cultured cells, including primary cells or skin cells differentiated from iPSCs, utilizing 3D bioprinting technology and skin-on-a-chip.[9–11] However, these technologies have been regarded as having limitations in terms of the structural complexity and cellular diversity required for the sophisticated reproduction of skin tissues. Notably, creating hair follicles in the skin graft has been a particularly challenging aspect of this endeavor.[12] Hair-bearing skin organoid (SkO) that is generated by self-organization of human induced pluripotent stem cells (iPSCs) has recently emerged as an excellent tool for closely mimicking multiple layered structures of human skin as well as a variety of skin appendages.[13] Recently, our group achieved significant progress in generating pure SkOs without off-target cartilages as well as planar sheet-like skin morphology.[14] These SkOs contain completely intact structures of the hair follicles consisting of outer wall structures such as dermal sheath (DS), outer root sheath (ORS) and inner root sheath (IRS), cellular components like melanocytes in the hair bulbs and dermal papilla cells (DP), and even hair shafts. Thus, they are advantageous for investigating the changes in the hair follicles in a 3D manner. In addition, this approach also enables analysis of spatial expression as well as interactions among diverse cell populations in the organoids.

Exosomes, referring to small extracellular vesicles released by various cell types, enable the intercellular communication by carrying bioactive molecules, such as proteins, nucleic acids, and lipids.[15] The exosomes hold significant promise as an alternative to cell-based therapy due to their ability to effectively stimulate target cells via direct fusion while possessing the characteristics and therapeutic effects of the parent cells.[16] However, the efficacy of exosomes can vary depending on the cell sources.[17] Given that exosomes derived from mesenchymal stem cells (MSCs) are able to regulate inflammation and promote extracellular matrix (ECM) synthesis, they have been utilized for treating various skin diseases, such as atopic dermatitis,[18,19] wound healing,[20,21] and skin aging.[22,23]

Here, we attempted to recapitulate an in *vitro* model of photodamage caused by sUV consisting of UVA (320–400 nm) and UVB (290–320 nm) radiation, especially on hair follicles by using iPSC-derived SkOs. Then, we assessed the effectiveness of the exosomes isolated from human umbilical cord blood-derived MSCs (UCB-MSCs), referred to as UCB-Exos, in mitigating hair follicle damage in the SkOs. Then, the mechanisms by which exosomes alleviated hair follicle damage were also investigated. We found that IκBα and NF-κB signaling was primarily linked to sUV-induced damage of hair follicles, which could be suppressed by treatment of UCB-Exos. Therefore, our SkOs containing hair follicles can be a valuable tool for studying the disease pathology as well as therapeutic mechanisms of drug candidates.

Methods

Human iPSC culture

This study was carried out in accordance with the approved guidelines of the Seoul National University Institutional Review Board (IRB No. 2211/003-013). The human iPSC line CMC003 was obtained from the National Stem Cell Bank of Korea (KSCB) for the generation of skin organoids. These iPSCs were maintained in Essential 8 media (Gibco, USA) on the dishes pre-coated with vitronectin (Gibco). The cells were passaged every 3–4 days using ReLeSR™ reagent (STEMCELL Technologies, Canada). Human iPSCs were cultured for up to 50–70 passages.

Generation of iPSC-derived human SkOs

SkOs were generated and cultured following the protocol as previously described.[14] Briefly, on day 0, 1200 iPSCs/well were seeded in Essential 8 medium with 20 μM ROCK inhibitor Y-27632 (Tocris, UK) in ultra-low attachment 96-well plate (Corning, USA) to generate uniform embryoid bodies (EBs). When the size of the EBs became 250 μm, the EBs were transferred into individual new ultra-low attachment 96-well plates in Essential 6-based differentiation medium containing 2% Matrigel (Corning), 10 μM SB431542 (Tocris), 4 ng/ml bFGF (Sigma-Aldrich,

USA), and 15 ng/ml BMP4 (Peprotech, USA) to initiate non-neural ectoderm induction. After 4 days of culture in non-neural ectoderm induction medium, 200 ng/ml LDN (Tocris), 50 ng/ml bFGF were added at 25 µl per well to induce cranial neural crest cell formation, and 15 µM CHIR99021 (Toscris), a Wnt signaling agonist, was co-treated to prevent off-target chondrogenic differentiation and increase the organoid diameter. On day 6 of differentiation, 75 µl of fresh E6 medium was added. Half of the medium was changed on days 8 and 10. On day 12, to induce self-assembly of the epidermis, all organoids were transferred into ultra-low-attachment 6-well plates and placed on an orbital shaker (SPL Life Science, Republic of Korea) in 3 mL of SkO maturation medium containing a 1:1 mixture of advanced DMEM-F12 and Neurobasal medium (Gibco) supplemented with 1× N-2 supplement (Gibco), 0.5× B-27 without vitamin A supplement (Gibco), 2-mercaptoethanol (Sigma-Aldrich), 1× GlutaMAX (Gibco). At approximately 85 days, each cyst-like SkO was cut into eight evenly sized portions, placed on polymerized collagen I (Corning) - coated transwell culture inserts, and maintained for 3–4 weeks in a humidified incubator (SPL Life Science). The maturation medium was changed every 2–3 days. To further induce epidermal maturation, the SkOs were transferred to a dry-conditioned incubator at 37 °C for an additional 6 days, and the medium was replaced daily.

Human skin sample preparation

Human skin samples were obtained from a healthy female (63 years old) through BIOHEAD (Seoul, Republic of Korea, BHF0303210). The samples were fixed with 4% paraformaldehyde in PBS and embedded in gelatin/sucrose solution for histologic and immunohistochemical analysis.

Histological analysis

SkOs were fixed in 4% paraformaldehyde in PBS overnight at 4°C. After washing with PBS more than three times, the organoids were pooled with 30 % sucrose solution overnight, embedded in a mixture of 10% gelatin and 30% sucrose solution, and then frozen at −80°C. After the organoids were cryosectioned into 10-µm thick, the sections were washed in PBS at 37 °C for 10 min. For hematoxylin and eosin (H&E) staining, sections were incubated in hematoxylin solution for 5 min and washed with 0.5% HCl in ethanol, followed by counterstaining with eosin for 1 min. For Masson's trichrome staining, the sections were re-fixed in Bouin's solution overnight at room temperature (RT). Then, the sections were incubated in Weigert's hematoxylin for 10 min, Biebrich scarlet-acid fuchsin for 5 min, and a mixture of phosphotungstic acid, phosphomolybdic acid and distilled water (1:1:2) for 10 min. Thereafter, slides were directly transferred to 2% aniline blue, incubated for 5 min, and washed with 1% acetic acid. After incubating with an increasing sequential ethanol series, the samples were mounted with Canada Balsam in xylene. Samples were visualized with an Olympus microscope and ProgRes CapturePro software (Olympus, Japan).

Immunohistochemistry analysis

The cryosectioned organoids were washed with PBS and permeabilized with sodium citrate (pH 6.0) at 95 °C for 5 min. After permeabilization, the samples were washed three times with PBS and blocked with 5% normal goat serum containing 0.1% Triton X-100 at RT for 1 h. The sections were incubated overnight with the primary antibodies diluted in 5% normal goat serum containing 0.2% Triton X-100 at 4°C (Additional file 2: Supplemental Table 1). After three washes with PBS, the sections were incubated with the following fluorescent secondary antibodies for an hour at RT: Alexa Fluor 488-labeled (A11008, A11001, Invitrogen, USA), 594-labeled (A11012, A11005, Invitrogen). Then, the nuclei were stained with DAPI (Invitrogen) for 15 min at RT. Finally, the sections were washed in PBS and mounted with a mounting solution (Dako, Denmark). Confocal images were captured by a confocal microscope (Eclipse TE200, Nikon, Japan) with the EZ-C1 3.8 program. To quantify the expression level of protein, mean fluorescence intensity (MFI) was measured in the segmented regions of the organoids using ImageJ (National Institutes of Health, USA). The number of cells in specific areas was manually counted by using ImageJ.

Modeling of sUV-induced photodamage

The sUV source was obtained from Q-Lab Corporation (Cleveland, OH, USA). The UVA-340 lamp is able to closely mimic a natural sUV.[24] The UVA-340 lamps emit radiation in the critical short wavelength region from 365 nm down to the solar cutoff of 295 nm, with a peak emission at 340 nm. A filter was employed to block UVC wavelengths below 290 nm. The proportion of UV-A (320–400 nm) and UV-B (280–320 nm) radiation produced by the UVA-340 lamp was measured with a UV meter: UV-A made up 94.5% of the total radiation, with 5.5% of UV-B. The sUV light dose was determined as 50 kJ/ m^2, according to the previous report[24] as well as our experimental results. Before sUV irradiation, SkOs were washed twice with PBS and subsequently exposed to sUV for 20 min, twice with a 2-h interval between exposures, resulting in a total of 50 kJ/ m^2 of sUV. These exposures were conducted at 2-day intervals for a total of three exposures.

RNA extraction and quantitative real-time polymerase chain reaction (qRT-PCR)

One piece of SkOs from each group was washed with PBS and lyzed in Nucleozol (Macherey-Nagel, Germany) for

total RNA extraction. Complementary DNA synthesis was conducted using a Superscript III First-Strand synthesis system kit (Invitrogen) according to the manufacturer's instructions. qRT-PCR analysis was performed with SYBR Green PCR Mix (Applied Biosystems, USA) on a 7500 Real-Time PCR system (Applied Biosystems). The relative mRNA expression of each target gene was quantified by the $2^{(\Delta\Delta \text{ threshold cycle})}$ ($2^{-\Delta\Delta CT}$) method and normalized to the housekeeping gene, glyceraldehyde-3-phosphate dehydrogenase (*GAPDH;* Supplemental Table 2).

Isolation of UCB-Exos

Human UCB-Exos were collected and purified from the culture medium. UCB-MSCs, obtained from a master cell bank, were cultured in a serum-free medium to boost exosome secretion. A conditioned medium containing secreted exosomes was collected and subjected to isolation of the exosomes through a three-step separation and purification process (adjacent flow filtration - ultracentrifugation - size exclusion chromatography). Initially, substances smaller than exosomes in the cultured medium were removed using Tangential Flow Filtration (TFF). Following this, centrifugation was employed to remove heavier debris through a process at 3000*g*, while a high-speed centrifugation process at 100,000*g* was utilized to eliminate lighter substances. Lastly, Size Exclusion Chromatography (SEC) was performed to selectively recover exosomes within a specific size range, thus yielding highly purified exosomes.

Transmission electron microscopy (TEM)

For morphological characterization, UCB-Exos were loaded on a glow-discharge carbon-coated copper grid. Then, the samples were stained with 2% uranyl acetate solution. After drying, the grid was subjected to TEM imaging (JEM1010, JEOL, Japan).

Nanoparticle tracking analysis (NTA)

The size of exosomes was measured by using a Nanosight NS300 (Malvern Panalytical Ltd, UK) instrument. To ensure that less than 100 exosomes were analyzed per flame, exosome samples were diluted with PBS and measured in triplicate between camera gain levels[12–15] (electronic image amplification).

SkO penetration assay

UCB-Exos were fluorescently labeled with ExoGlow-protein EV Labeling Kit (System Biosciences, USA) according to the manufacturer's protocol. Labeled exosomes were applied to the skin organoids and incubated for up to 24 h. To assess the internalization of exosomes, the skin organoids were fixed with 4% paraformaldehyde at indicated time points 9, and 24 h.

Western blot analysis

Protein samples were prepared using protein lysis buffer Pro-prep (Intron Biotechnology, Republic of Korea). The nuclear and cytosolic fraction was respectively isolated using NE-PER Nuclear and Cytoplasmic Extraction Reagents (Thermofisher Scientific). The 20 µg of proteins were separated by sodium dodecyl sulfate-polyacrylamide gel electrophoresis (SDS-PAGE) and transferred to polyvinylidene difluoride (PVDF) membranes. The membranes were blocked with a 3% bovine serum albumin solution at RT for an hour and then incubated on an agitator with the primary antibodies at 4°C overnight (Supplemental Table 1). Membranes were washed and incubated with secondary antibodies (G21040, G21234, Invitrogen) at RT for 1 h. Each band was detected with an enhanced chemiluminescence (ECL) detection kit (Cytiva, USA).

Enzyme linked immunosorbent assay (ELISA)

The secretion of IL-1β, IL-6, and TNF-α from the SkOs was quantified using human IL-1β Quantikine ELISA, IL-6 Quantikine ELISA and TNF-α Quantikine ELISA (DLB50, D6050, DTA00D, R&D Systems, USA). The culture supernatant was collected and centrifuged at 2000 rpm for 5 min to eliminate cell debris. The concentration of each cytokine was determined in accordance with the manufacturer's instructions.

Inhibition of NF-κB pathway

For suppression of NF-κB signaling, the SkOs were preconditioned with 15 µM of BAY11-7082 for 48 h (HY-13453, MedChem Express, USA). Then, the SkOs were stimulated with sUVs, followed by additional treatment of BAY11-7082 for 24 h. Then, each SkO was subjected to further analysis (e.g. Western blot, ELISA, and immunohistochemistry analysis).

Statistical analysis

Sample size (n) represents the number of biologically independent replicates. At least three independent experiments were conducted. All values in the graphs are presented as mean ± standard deviation (SD). All graphs were generated using GraphPad Prism version 10.0. Statistical analysis was performed by unpaired two-tailed *t*-test, two-way ANOVA with post-hoc Bonferroni's test, and one-way ANOVA with Tukey's post-hoc test for multiple comparisons, as indicated in each figure legend. Statistical significance was indicated as follows: $*p < 0.05$; $** p < 0.01$; $*** p < 0.001$. An exact p-value for each data was given in each figure legend.

Results

Characterization of iPSC-derived hair-bearing SkOs

The human SkOs generated were from iPSCs as previously reported[14] (Figure 1(a)). After iPSC-derived EBs were differentiated into the surface ectoderm, the cyst-like organoids were transferred to a maturation medium on day 14. After 8 weeks of maturation, epidermis-dermis layers were organized in the SkOs. After 10 weeks of maturation, hair follicles began to form within the SkOs. When the confluency of the hair follicles reached 70~80%, ALI culture was performed to create a more physiological environment for SkOs. After 28 days of ALI culture, fully mature SkOs containing elongated hair follicles, hair shafts, and adipocytes were obtained (Figure 1(b)). In addition, the SkOs exhibited histologically similar structures to human skin tissue, characterized by multiple skin layers, including a stratified epidermis and fat-rich dermis with hair follicles. (Figure 1(c)). Specifically, the expression of mature epidermal markers, such as Loricrin, Filaggrin, and KRT10, as well as dermal markers like collagen type 3 and Vimentin was confirmed in the corresponding layers of the SkOs, which closely resembled those of adult skin tissues (Figure 1(d)). Among dermal layers in SkOs, hair follicle structures were further investigated (Figure 1(e) and (f)). At the outermost layer of the hair follicles, the DS expressing α-SMA was observed. The ORS expressing KRT17 and KRT5, the IRS expressing KRT71, and the innermost cortex expressing AE13 were also identified (Figure 1(g)). In addition to wall structures, the presence of essential components for hair formation was confirmed. For instance, NFATc1+ hair follicle stem cells resided in a specialized area known as the bulge. Hair matrix cells expressing Ki67 and p63 and dermal papilla cells (DP) expressing SOX2 were also identified in the hair follicles (Figure 1(h)). Taken together, these results indicated that we successfully established hair follicle-bearing SkOs which were highly similar to human skin.

Modeling of sUV-induced skin damage in SkOs

There are two different types of sUV reaching the skin, UV-A and UV-B. It has been known that UV-A penetrates from the epidermal layer of the skin to the deepest layer of the dermis, while UV-B can only penetrate the epidermis and the top of the dermis. Exposure to sUV can lead to sunburn and other signs of aging, such as pigmentation, by destroying ECM components and the major proteins of the skin.[25] To mimic sUV-induced skin damage in vitro, SkOs were irradiated by a combination of UV-A and B, at 2-day intervals for a total of three exposures (Figure 2(a)). First, the effects of different doses of sUV on SkOs were investigated. As a result, a high dose, 75 kJ/m², of sUV caused exfoliation of the whole epidermal layer in SkOs, indicating that the structural integrity of the skin was significantly compromised (Supplemental Figure S1A). immunofluorescence staining results revealed that the degree of dermal impairment induced by 50 kJ/m² of sUV was comparable to the damage caused by 75 kJ/m² of sUV, while 25 kJ/m² of sUV did not cause significant damage to the SkOs (Supplemental Figure S1B and C). Therefore, 50 kJ/m² of sUV was determined to be an optimal dose for inducing photodamage in SkOs. After sUV exposure, there was a significant increase in epidermal thickness and the number of sunburn cells that were characterized by fragmentation or condensation of the cell nucleus in both epidermal and dermal layers of the SkOs (Figure 2(b) and (c) and Supplemental Figure S1D and E). In addition, the number of melanocytes in the epidermis and hair follicles was also increased compared to control SkOs, suggesting the pigmentation of the skin (Supplemental Figure S1F and G). Notably, we found that sUV also affected the outermost layer of the epidermis in SkOs, which served as the skin's protective barrier. The mRNA expression of the genes related to the skin barrier, *Filaggrin* and *Loricrin*, was significantly decreased in the sUV-exposed SkOs, suggesting the dysfunction of skin barriers after irradiation (Figure 2(d)). Consistently, the proteins forming the epidermal barrier, such as Filaggrin, Loricrin and CK10, were remarkably downregulated in the epidermis of sUV-exposed SkOs compared to that of control SkOs (Figure 2(e) and (f)). Furthermore, the influence of sUV also extends into the deeper dermal layer of SkOs. The density of collagen fibers was markedly reduced in the dermal layer of sUV-exposed SkOs (Figure 2(g) and (h)). Quantitative PCR analysis also demonstrated a significant decrease in *COL1A1* expression and an increase in matrix metalloproteinase-1 (*MMP-1*), an enzyme responsible for direct degradation of the ECM fibers,[26] in sUV-exposed SkOs compared to control SkOs (Figure 2(i)). In particular, a notable decrease in type I collagen expression and an increase in MMP-1 expression were particularly observed in the dermal layer of sUV-exposed SkOs (Figure 2(j) and (k)). Based on these results, the sUV reaching the epidermal and dermal layers provoked total skin damage in SkOs. Therefore, we successfully established in vitro conditions to recapitulate sUV-induced photodamage in SkOs.

SUV induces structural damage and pro-inflammatory responses in the hair follicles of SkOs

Next, the effects of sUV exposure on skin appendages in the dermis of the SkOs were investigated. The results showed a decrease in the marker expression of keratinocytes that constitute the outer layer of hair follicles in the SkOs (Figure 3(a) and (b)). Furthermore, there was a significant increase in apoptotic cells in the SkOs,

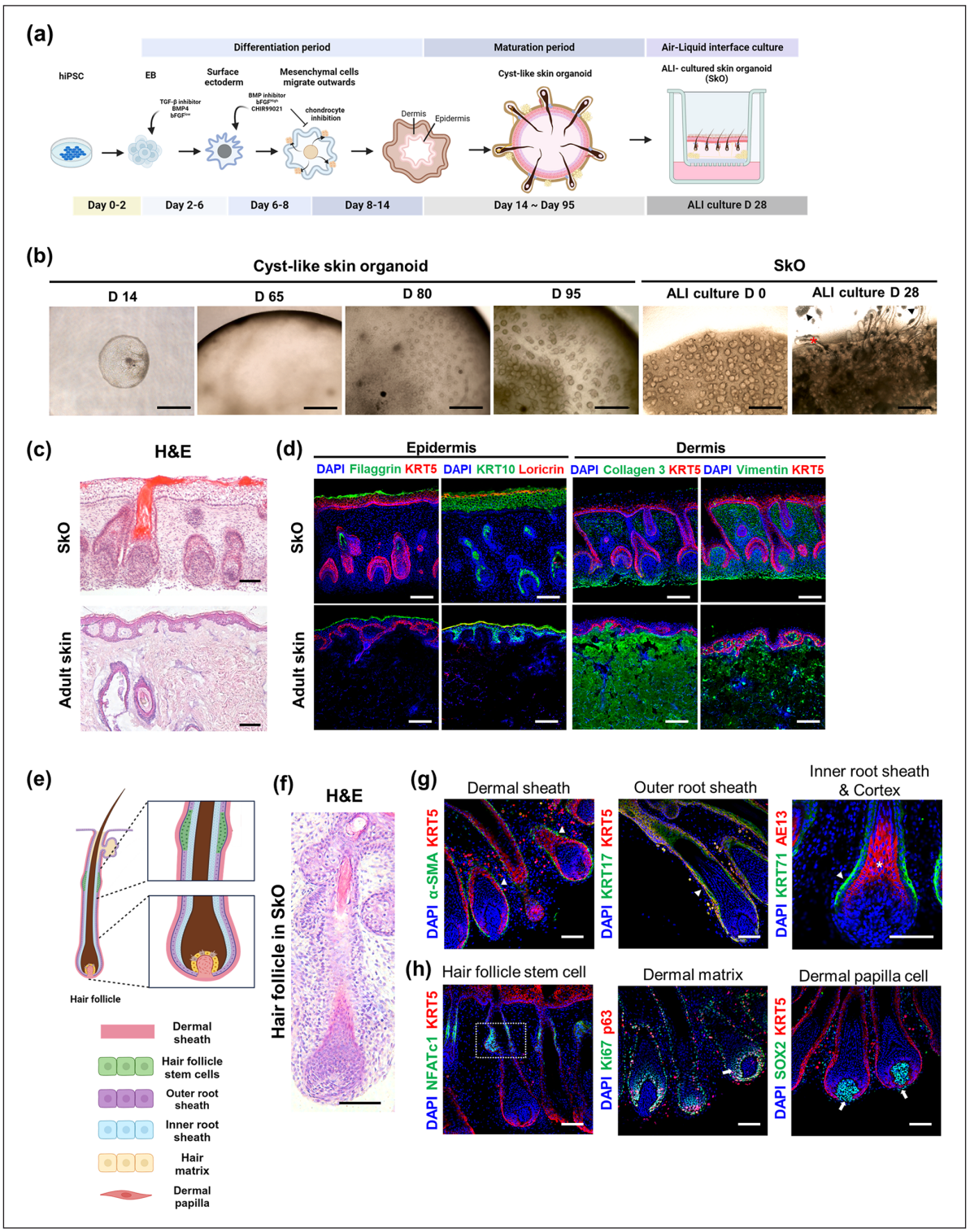

Figure 1. Generation of human SkOs with hair follicles: (a) schematic diagram of the protocols for generating human SkOs, (b) Bright-field images of generated SkOs on days 14, 65, 80, and 95, and the SkOs subjected to ALI culture on days 0 and 28. Note fully mature SkOs with elongated hair follicles (red asterisk) and adipocytes (arrowhead). Scale bar, 1 mm, (c) H&E staining of SkOs and human adult skin showing the multi-layered structures of the skin. Scale bar, 100 μm, (d) Representative confocal images of the SkOs and human adult skin in each group stained with the epidermal markers (Filaggrin, KRT10: green, KRT5, LOR: red) and dermal markers (Collagen 3, Vimentin: green). Nuclei were stained with DAPI (blue). Scale bar, 100 μm, (e) Illustration of follicular structures, (f) H&E staining of hair follicles in the SkOs. Scale bar, 50 μm, (g) Representative confocal images of the SkOs stained with each structural component of hair follicles; Dermal sheath (α-SMA: green; allow), outer root sheath (KRT17: green, KRT5: red; arrow), inner root sheath (KRT71: green; arrow) and cortex (AE13: red; asterisk). Scale bar, 50 μm, and (h) Representative confocal images of the SkOs stained with markers of each cell type; Hair follicle stem cell (NFATc1: green, KRT5: red), hair matrix cell (Ki67: green, p63: red) and dermal papilla cell (SOX2: green). Scale bar, 50 μm.

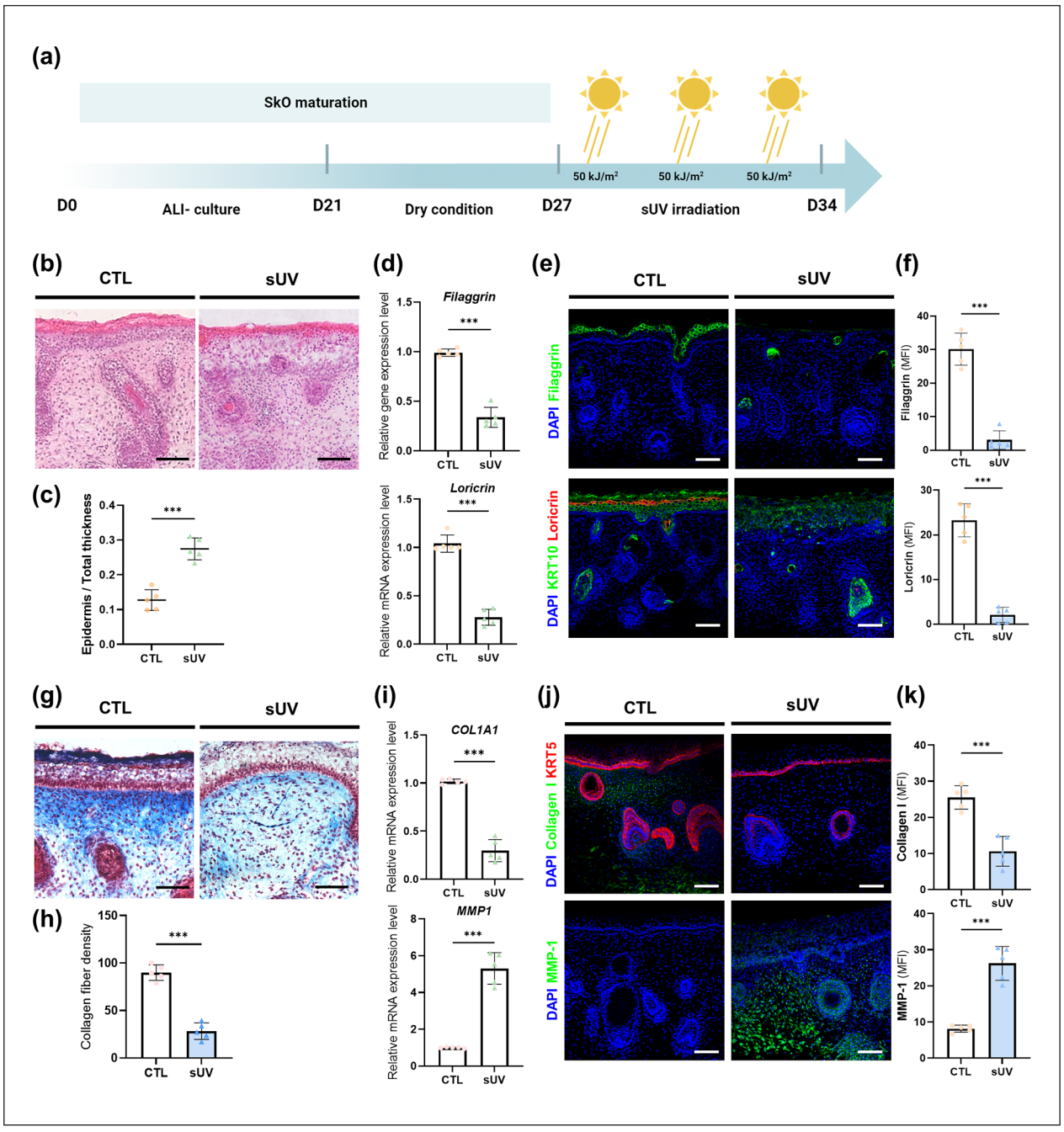

Figure 2. Simulating sUV-induced skin damage in the SkOs: (a) schematic diagram of the induction of sUV damaged skin model in SkOs, (b) H&E staining of control SkOs and sUV-exposed SkOs. Scale bar, 50 μm, (c) quantification of the thickness of epidermis normalized to the thickness of the entire skin ($n = 5$), (d) qRT-PCR of skin barrier related genes Filaggrin and Loricrin in control and sUV-exposed SkOs ($n = 5$), (e) representative confocal images of the control and sUV-exposed SkOs stained with Filaggrin (green, top), and KRT10 (green, bottom) and Loricrin (red, bottom). Nuclei were stained with DAPI. Scale bar; 100 μm, (f) mean fluorescence intensity (MFI) of Filaggrin and Loricrin in the randomized fields of stained sections in each group ($n = 5$), (g), (h) Masson's trichrome staining (g) of the SkOs in each group and quantification (h) of collagen fiber density (blue) in the dermis. Scale bar, 100 μm ($n = 5$), (i) qRT-PCR analysis of COL1A1 and MMP1 in control and sUV-exposed SkOs ($n = 5$), (j) Representative confocal images of the control and sUVexposed SkOs. Top panel: COL1 (green), KRT5 (red), and DAPI (blue), bottom panel: MMP-1 (green) and DAPI (blue). Scale bar, 100 μm. Quantitative data were presented as a mean ± SD. Statistical differences between the groups were determined by unpaired student's *t*-test (***$p < 0.001$).

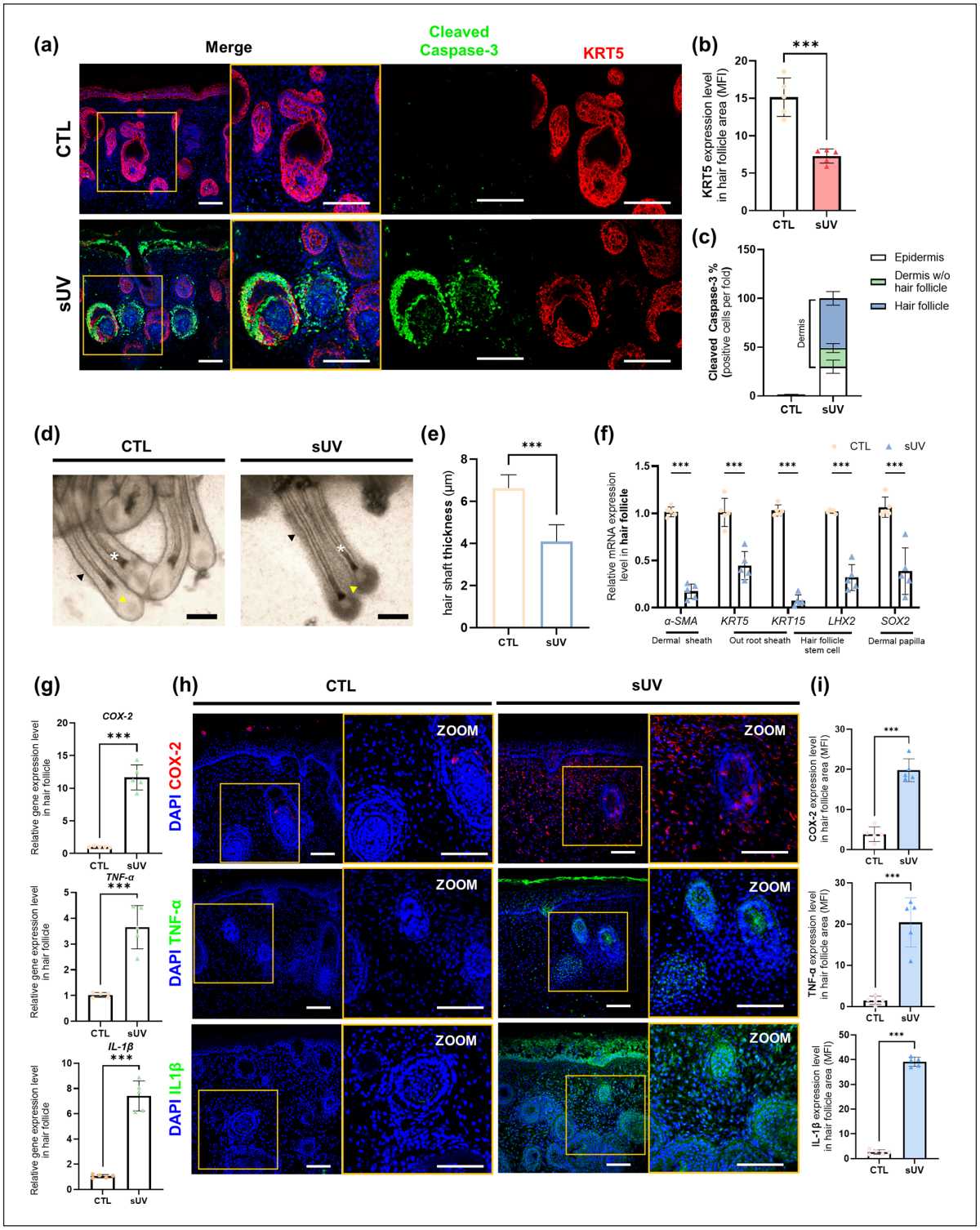

Figure 3. Modeling of sUV-induced photodamage on the hair follicles in the SkOs: (a) representative confocal images of control and sUV-exposed SkOs for apoptosis stained with Cleaved-Caspase 3 (green) and KRT5 (red). Scale bar, 100 μm, (b) MFI of KRT5 in hair follicles of control and sUV-exposed SkOs ($n = 5$), (c) quantification of Cleaved Caspase-3 positive cells depending on their location in the SkOs, (d) bright-field images of hair follicles in control SkOs and sUV-exposed SkOs. Hair shafts (asterisk), ORS (black arrow), and DP (yellow arrow). Scale bar, 100 μm, (e) quantification of the thickness of the hair shafts in each group ($n = 5$), (f) qRT-PCR analysis of genes related to follicular structures including DS, ORS, HFSC, and DP in the hair follicles isolated from SkOs ($n = 5$), (g) qRT-PCR analysis of COX-2, TNF-α, and IL-1β in hair follicles of control and sUV-exposed SkOs ($n = 5$), (h) representative confocal images and magnified images of the control and sUV-exposed SkOs for pro-inflammatory cytokines, COX-2, TNF-α, and IL-1β. Scale bar, 100 μm, (i) MFI of COX-2, TNF-α, and IL-1β in hair follicles of control and sUV-exposed SkOs ($n = 5$). Quantitative data were presented as a mean ± SD. Statistical differences between the groups were determined by unpaired, two-tailed student's *t*-test (b, e, g) and two-way ANOVA with post-hoc Bonferroni's test (f) (***$p < 0.001$).

particularly co-localized with cells expressing KRT5 in the hair follicle (Figure 3(a) and (c)). The bright field images also showed that the DS and ORS of the hair follicle were markedly destroyed, and the hair shaft became relatively thinner in the sUV group compared to the control group, indicating the transition from the anagen phase to catagen phase of hair follicles following sUV exposure (Figure 3(d) and (e)). Therefore, to thoroughly compare the degree of hair follicle damage, hair follicles were isolated from each skin organoid and subjected to qRT-PCR analysis. The gene expression of DS marker (*a-SMA*), ORS markers (*KRT5*, *KRT15*), hair follicle stem cells markers (*KRT15*, *LHX2*), and DP marker (*SOX2*) was significantly reduced in the sUV group, indicating that sUV radiation penetrating the dermal layer could cause deteriorating effects to hair follicles (Figure 3(f)). sUV irradiation is known to stimulate the release of pro-inflammatory cytokines in the skin tissues, leading to skin inflammation and consequent skin damage.[27] Accordingly, we investigated whether sUV exposure could also affect the hair follicles and induce inflammatory responses in the dermis of SkOs. First, the gene expression of pro-inflammatory cytokines, such as *COX-2*, *TNF-*α, and *IL-1*β was significantly upregulated in the hair follicles of sUV-exposed SkOs (Figure 3(g)). Then, immunofluorescence analysis was conducted to identify localized inflammatory responses in the SkOs. The results showed that the increased production of pro-inflammatory cytokines was evident within the hair follicles of sUV-irradiated SkOs despite being expressed throughout the skin layers (Figure 3(h) and (i)). These results suggested that sUV radiation caused structural damage and inflammatory responses in the hair follicles of the SkOs. Collectively, our findings demonstrated that exposure to sUV could sensitize and destroy not only the skin tissues but also the hair follicles responsible for hair growth.

Characterization of human UCB-Exos penetrating into the SkOs

Furthermore, we explored the utility of sUV-damaged SkOs as a model for studying mechanisms of action of potential drugs for photodamage. Currently, the exosomes derived from hUCB-MSCs have been considered a therapeutic drug candidate for various skin problems due to their ability to promote skin regeneration and reduce skin inflammation.[22,28] In this context, we investigated the effects of the UCB-Exos on photodamage by using the sUV-exposed SkOs. The exosomes isolated from human UCB-MSCs were round-shaped with an average diameter of 121 ± 39.4 nm, which was evidenced by TEM and NTA analyses (Figure 4(a) and (b)). The purity of the UCB-Exos, calculated by the ratio of particle counts to protein concentration, was determined to be more than 2.6×10^9 particles/μg (Figure 4(c)). Western blot analysis confirmed the expression of exosomal markers CD9, CD63, and TSG101 in the UCB-Exos (Figure 4(d)). Furthermore, flow cytometry results showed the positive expression of exosomal markers, such as CD9 (80.76%), CD63 (65.65%), and CD81 (93.46%), in the UCB-Exos, while non-exosomal markers, GM130 (0.22%), Cytochrome C (5.04%), and Calnexin (0.65%) were negatively expressed (Figure 4(e)–(g)). To visualize the penetrating UCB-Exos into the SkOs, UCB-Exos labeled with green fluorescent Exogreen was applied. After 9 h, UCB-Exos were primarily localized in the epidermis of SkOs. However, 24 h after UCB-Exos treatment, they penetrated into the dermal layer of SkOs, indicating that the UCB-Exos could be internalized by the dermis through the epidermis (Figure 4(f) and (g)).

UCB-Exos ameliorated the sUV-induced hair follicle damage in SkOs

To determine the optimal concentration of UCB-Exos for alleviating sUV-induced damage to SkOs, SkOs were treated with different concentrations of UCB-Exos after 2 h of sUV exposure, and this cycle was repeated three times (Figure 5(a)). The results demonstrated that UCB-Exos treatment effectively reduced SkO damage in a dose-dependent manner.

Specifically, treatment of more than 1×10^8 particles of UCB-Exos effectively mitigated cell apoptosis within the dermal layer, including hair follicles, in the SkOs induced by sUV exposure (Supplemental Figure S2A and B). However, a more significant effect on alleviating the inflammatory response was observed at a concentration of 1×10^9 particles of UCB-Exos (Supplemental Figure S2C). Based on these results, we determined that at least 1×10^9 particles of UCB-Exos are required to fully exert their beneficial effects in inhibiting cell apoptosis, restoring skin barrier functions, and regulating the secretion of inflammatory cytokines. Furthermore, UCB-Exos (1×10^9) treatment effectively reduced epidermal thickness (Supplemental Figure S3A and B) and alleviated the disruption of the barrier proteins (Filaggrin and Loricrin), indicating the amelioration of sUV exposure-induced epidermal damage in the SkOs (Supplemental Figure S3C-E). In addition, the density of collagen fibers, which had decreased after sUV exposure, was restored (Supplemental Figure S3F and G). Consistently, not only reduced *MMP-1* expression but augmented *COL1A1* expression was identified in the UCB-Exos-treated SkOs compared to the Vehicle control group (Supplemental Figure S3H). Immunofluorescence analysis also revealed that the dermis of UCB-Exos-treated SkOs retained higher levels of collagen fibers and reduced expression of MMP-1, suggesting that UCB-Exos suppressed collagen breakdown in sUV-damaged SkOs (Supplemental Figure S3I and J). More importantly, we then focused on the effects of UCB-Exos on the hair follicles within the SkOs. The apoptotic levels (Cleaved Caspase-3$^+$) were reduced, while the

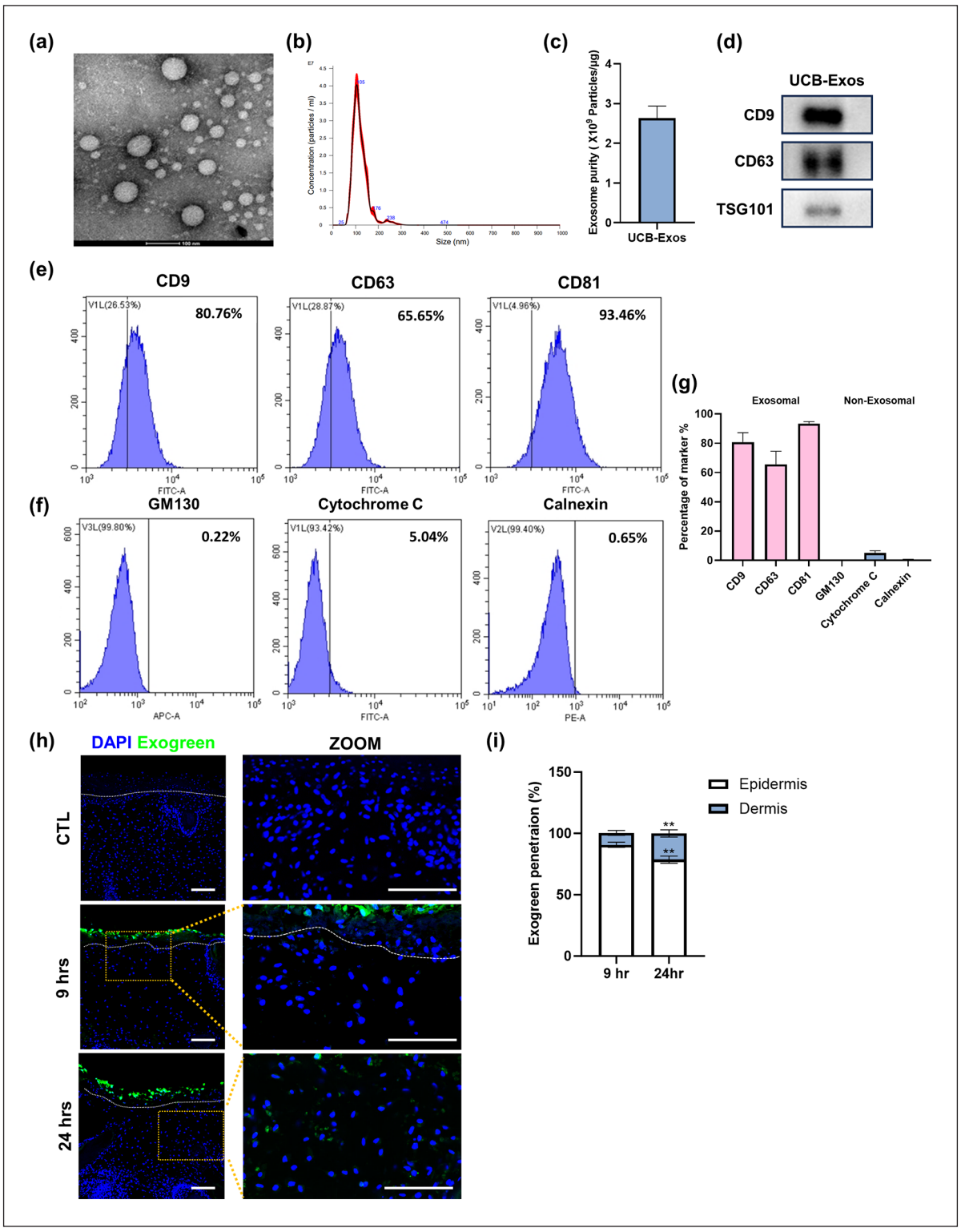

Figure 4. Characterization of exosomes-derived UCB-MSCs: (a) TEM analysis of UCB-Exos for morphological characterization. Scale bar, 100 nm. (b) Particle diameter distribution detected by NTA. The mean particle diameter was 121 ± 39.4 nm, (c) exosome purities (exosome particles/μg of protein) from UCB, (d) Western blotting of exosomal markers, CD9, CD63, and TSG101, in the UCB-Exos, (e) flow cytometry analysis of exosome-positive markers, CD9, CD63, and CD81 in the UCB-Exos, (f) flow cytometry results of exosomenegative markers GM130, Cytochrome C, and Calnexin in the UCB-Exos, (g) quantification of flow cytometry results for exosome-positive and negative marker ($n = 3$), (h) representative confocal images of fluorescent Exogreen-labeled UCB-Exos penetrated into SkOs after 9 and 24 h. Scale bar, 100 μm, and (i) quantification of Exogreen detected in epidermis and dermis, respectively, normalized to total green MFI ($n = 3$). Quantitative data were presented as a mean ± SD. Statistical differences between the groups were determined by unpaired, two-tailed student's *t*-test (**$p < 0.01$).

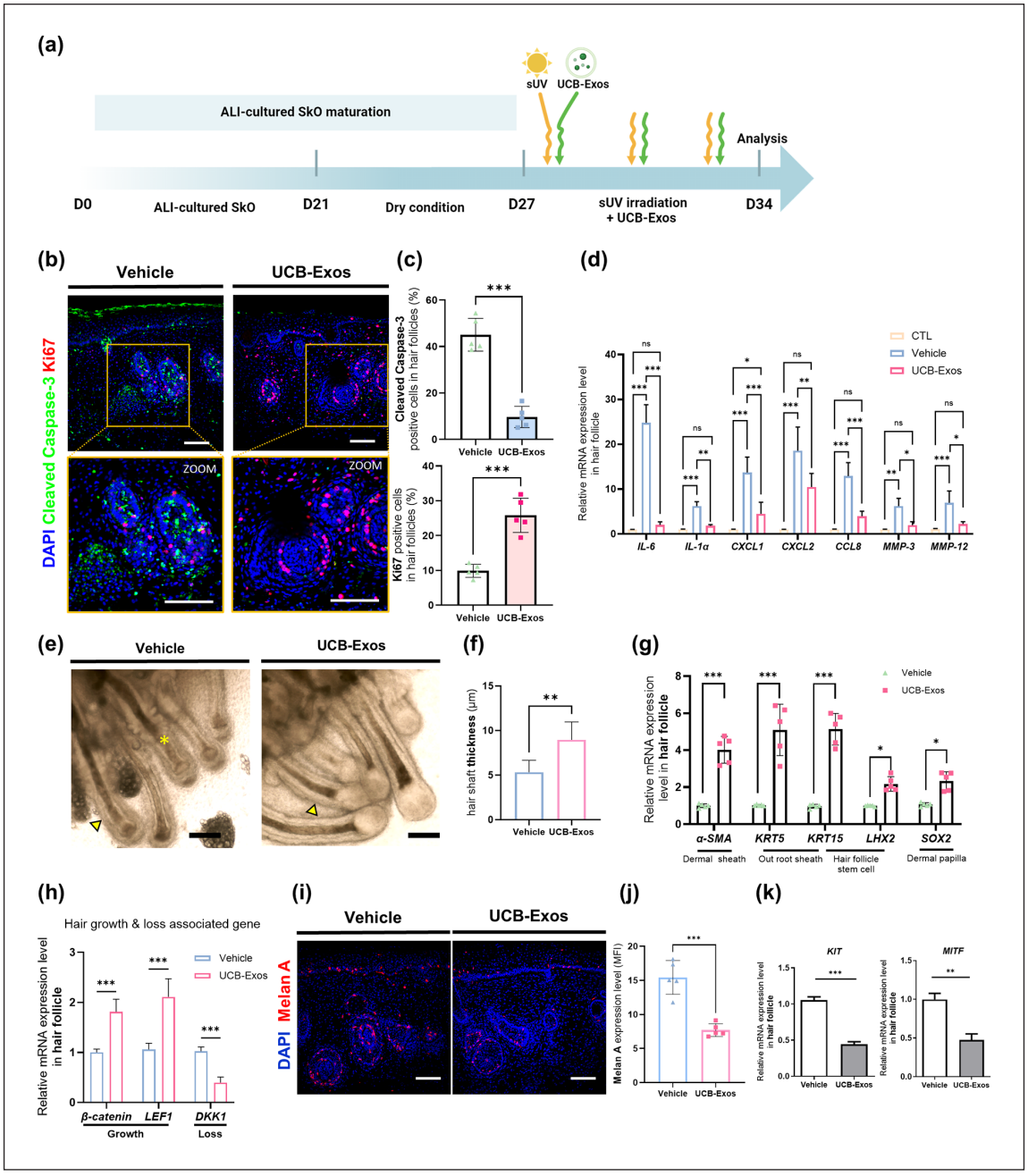

Figure 5. UCB-Exos attenuated the damage of hair follicles upon sUV exposure: (a) schematic diagram of UCBExos treatment in the sUV-exposed SkOs, (b) immunostaining of apoptosis marker, Cleaved Caspase-3 (green) and proliferation marker, Ki67 (red) in Vehicle- or UCB-Exos-treated SkOs. DAPI (blue) was used for nuclei staining. Scale bar, 100 μm, (c) quantification of Cleaved Caspase-3-positive cells and Ki67-positive cells in hair follicles of SkOs ($n = 5$), (d) qRT-PCR of SASP-related genes in the hair follicles isolated from Vehicle and UCB-Exos treated SkOs upon sUV exposure ($n = 5$), (e) bright-field images of hair follicles and hair shafts in Vehicle- or UCB-Exos treated SkOs. Note the hair shafts exhibiting a transition to catagen phase (yellow asterisk) and disrupted ORS (yellow arrowhead) in the Vehicle group, in contrast to restored hair shafts (white asterisk) and ORS (black arrowhead) in the UCB-Exos group. Scale bar, 100 μm, (f) quantification of the thickness of hair shafts in the Vehicle group and UCB-Exos treated group ($n = 5$), (g) qRT-PCR of hair follicle structure (DS, ORS, HFSC, and DP) related genes on isolated only hair follicles from sUV exposed and UCB-Exos treated SkOs ($n = 5$), (h) qRT-PCR analysis of genes associated with hair growth and loss in the only hair follicles respectively isolated from Vehicle- or UCB-Exos treated SkOs ($n = 5$), (i), (j) representative confocal images (i) and MFI quantification (j) of melanocytes stained with Melan A (red) in Vehicle-treated SkOs and UCB-Exos-treated SkOs. Scale bar, 100 μm. (n = 5), (k) qRT-PCR analysis of genes linked to melanin formation, KIT and MITF, in the hair follicles isolated from Vehicle- or UCB-Exos-treated SkOs ($n = 5$). Quantitative data were presented as a mean ± SD. Statistical differences between the groups were determined by unpaired, two-tailed student's *t*-test ((c), (f), (j), (k)) and two-way ANOVA with posthoc Bonferroni's test ((d), (h)) (*$p < 0.05$. **$p < 0.01$. ***$p < 0.001$, ns; not statistically significant).

number of regenerating cells ($Ki67^+$) increased in the hair follicles of the UCB-Exos group (Figure 5(b) and (c)). Moreover, UV-induced senescent keratinocytes and fibroblasts, which primarily compose the hair follicles, have been reported to secrete MMPs and inflammatory cytokines, known as the senescence-associated secretory phenotype (SASP).[29,30] We confirmed that the genes associated with SASP were significantly downregulated in the hair follicles in the UCB-Exos group, indicating a less aged and healthier state (Figure 5(d)). Thus, these combined results suggested that UCB-Exos effectively mitigated sUV-induced cell death and senescence in the hair follicles while promoting hair follicle regeneration. The sUV-induced damages of hair follicles, such as shrunk hair bulbs and destruction of outer walls like DS and ORS, were distinctly recovered in the UCB-Exos-treated group (Figure 5(e) and (f)). Moreover, abnormal catagen entry of hair shafts, as evidenced by the detachment of the hair shaft from the DP to be regressed, in the Vehicle group was restored after UCB-Exos treatment (Figure 5(e)). Consistently, the expression of genes related to the structural components of hair follicles was upregulated in the UCB-Exos group (Figure 5(g)). Furthermore, hair growth-associated genes, such as β-catenin and LEF1, were upregulated, whereas the hair loss-associated gene, DKK1, was downregulated in the UCB-Exos group, suggesting that UCB-Exos rescued the hair-forming ability of SkOs (Figure 5(h)). Meanwhile, melanocytes were also affected by UCB-Exos treatment. We observed that not only the number of melanocytes decreased in both the epidermis and hair follicles (Figure 5(i) and (j)), but also the expression of genes related to melanocyte development and pigmentation, *KIT* and *MITF*, was reduced in the sUV-exposed SkOs after UCB-Exos treatment (Figure 5(k)). Taken together, we proved the therapeutic potential of UCB-Exos in ameliorating skin damage and enhancing hair follicle regeneration in sUV-exposed SkOs.

UCB-Exos attenuated IκB/NF-κB-mediated inflammatory responses in sUV-exposed hair follicles

Numerous studies have argued that exposure to sUV radiation induces cell death through activating inflammatory cascades in the skin.[31,32] Above all, NF-κB has been known to play a pivotal role in regulating the expression of immune mediators. In its inactive state, NF-κB is bound to an inhibitory protein known as IκBα in the cytoplasm, forming the NF-κB-IκB complex. When activated by external stimuli like inflammatory cytokines or cellular stress, the IκB family proteins are phosphorylated and subsequently degraded, triggering the release of NF-κB from the NF-κB-IκB complex. The liberated NF-κB is translocated to the cell nucleus, where it promotes the transcription of genes involved in the inflammation and drives cytokine production.[33] Considering this, we investigated whether IκB-dependent NF-κB activation mediated inflammatory responses in the hair follicles.

We found that sUV markedly induced phosphorylation of IκBα and subsequent degradation of IκBα in the cytosol fraction of the SkOs. This led to disruption of the NF-κB-IκB complex, and thereby causing NF-κB to be activated and translocated to the nucleus, as evidenced by increased NF-κB expression in the nuclear fraction of the sUV-exposed SkOs. After treatment of UCB-Exos in sUV-exposed SkOs, reduction of not only IκBα phosphorylation but IκBα degradation was observed while the nuclear translocation of NF-κB was also suppressed (Figure 6(a) and (b)). Immunofluorescence staining also revealed localized expression of IkBα and the active form of NF-κB, phospho-NF-κB (p-NF-κB), in the cells that compose hair follicle structures. Generally, the hair follicle is composed of keratinocytes and fibroblasts, both of which play crucial roles in skin inflammatory response.[34,35] Remarkably, we observed a drastic suppression of IkBα, which is normally expressed throughout the entire hair follicle, particularly in the ORS keratinocytes in the vehicle group (Figure 6(c) and (d)). Accordingly, sUV exposure induced a marked increase in p-NF-κB expression the ORS and matrix of hair follicles (Figure 6(c) and (d)). The nuclear translocation of p-NF-κB was also increased in those structures in sUV-induced SkOs compared to those in the control SkOs, indicating the activation of NF-κB following sUV exposure. Of note, the NF-κB-mediated inflammatory responses mainly occurred in the hair follicles rather than in dermal fibroblasts (Supplemental Figure S3A-B). Meanwhile, the epidermis of SkOs, which is the topmost layer exposed to sUV, was also inflamed, likely extending to the dermal layers and indirectly damaging hair follicles.[36,37] (Supplemental Figure S3C and D). These expression patterns of IκBα and NF-κB were effectively reversed by UCB-Exos treatment (Figure 6(c) and (d)). Furthermore, the mRNA expression of pro-inflammatory genes, *TNF*-α and *IL-6*, was significantly reduced in the isolated hair follicles following UCB-Exos treatment (Figure 6(e)). The protein levels of TNF-α and IL-6, which were high throughout the hair bulbs of the Vehicle group, notably decreased in the matrix region upon treatment of UCB-Exos (Figure 6(f) and (g)) This was consistently reflected in the secretomes of TNF-α and IL-6 in the SkOs as confirmed by ELISA (Figure 6(h)). Overall, these results suggested that UCB-Exos mitigated pro-inflammatory responses, particularly in fibroblasts and keratinocytes residing in the hair follicles, by inhibiting IκB degradation and NF-κB activation, which was induced by sUV exposure.

Suppression of NF-κB signaling mediated the therapeutic efficacy of exosomes on hair follicle photodamage

To assess the direct effects of UCB-Exos in alleviating sUV-induced damage through NF-κB activation, we

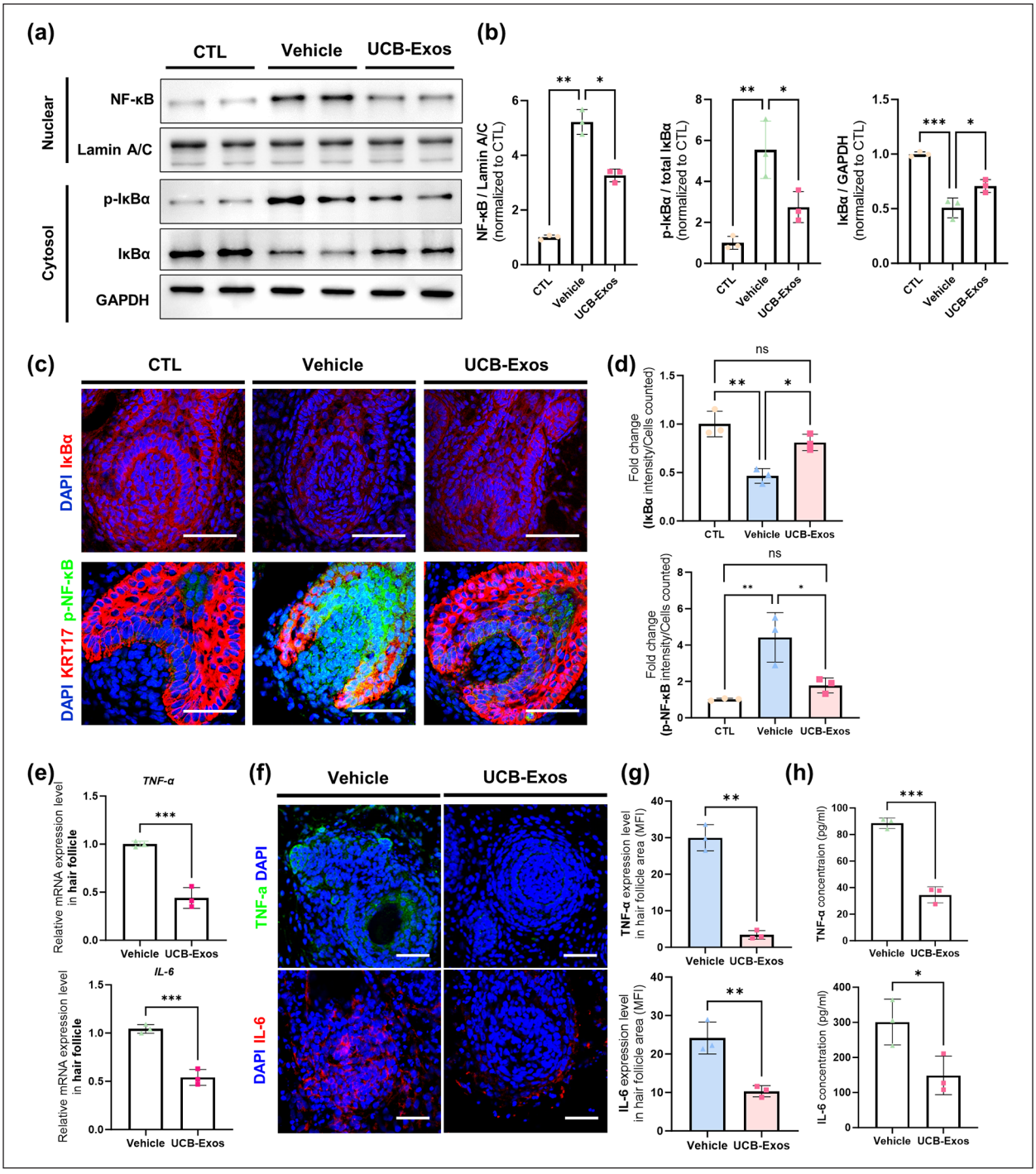

Figure 6. Suppression of pro-inflammatory responses in sUV-exposed hair follicles by UCB-Exos: (a) Western blot analysis of the SkOs without sUV exposure (CTL), treated with vehicle after sUV exposure (Vehicle), and treated with UCB-Exos after sUV exposure (UCB-Exos). After obtaining each nuclear and cytosol fraction, NF-κB expression in nucleus as well as p-IκBα and total IκBα expression in cytoplasm was shown. The loading control of nuclear fraction was Lamin A/C and that of cytosol fraction was GAPDH, (b) quantification of NF-κB levels normalized to nuclear Lamin A/C expression, p-IκBα levels normalized to total IκBα levels, and IκBα was normalized to cytosol GAPDH expression ($n = 3$), (c) representative confocal images of hair follicles stained with IκBα (red, top), p-NF-κB (green, bottom), and KRT17 (red, bottom) in the CTL, Vehicle and UCB-Exos group. Nuclei were stained with DAPI. Scale bar; 50 μm, (d) MFI quantification of IκBα (top) and p-NF-κB (bottom) normalized to cell numbers in each group ($n = 3$), (e) qRT-PCR analysis of TNF-α and IL-6 in the hair follicles isolated from Vehicle group and UCB-Exos group ($n = 3$), (f), (g) representative confocal images (f) and MFI quantification (g) of the hair follicles stained with TNF-α (green, top) and IL-6 (red, bottom). Scale bar, 50 μm ($n = 3$), (h) secretion of proinflammatory cytokines, TNF-α and IL-6, from vehicle- or UCB-Exos-treated SkOs was quantified by ELISA ($n = 3$). Quantitative data were presented as a mean ± SD. Statistical differences between the groups were determined by unpaired student's *t*-test and ordinary one-way ANOVA with post-hoc Tukey test (*$p < 0.05$. **$p < 0.01$. ***$p < 0.001$, ns; not statistically significant).

treated sUV-damaged organoids with the NF-κB inhibitor BAY11-7082. It is known for inhibiting the degradation of IκBα units, thereby suppressing the translocation of NF-κB into the nucleus, preventing further activation of NF-κB signaling.[38] Following BAY11-7082 treatment, sUV-damaged SkOs exhibited a reduction in phosphorylated IκBα, resulting in the inhibition of IκBα degradation and subsequent downregulation of nuclear translocation of NF-κB (Figure 7(a) and (b)). Similarly, sUV-exposed SkOs supplemented with UCB-Exos also displayed a significant reduction in IκBα phosphorylation, followed by decreased IkBα degradation and NF-κB activation, comparable to the effects of BAY11-7082. Notably, co-treatment with BAY11-7082 and UCB-Exos synergistically reduced both NF-κB and phospho-IκBα levels. As expected, the expression of IL-6 was positively correlated with the NF-κB expression level (Figure 7(a) and (b)). Furthermore, we evaluated the secretion of pro-inflammatory cytokines, IL-6, TNF-α, and IL-1β, which were increased by sUV exposure (Figure 7(c)). While there was no significant difference in the secretion of IL-6 and TNF-α between the SkOs treated with BAY11-7082 and those treated with UCB-Exos, a significant decrease in TNF-α and IL-1β levels was observed in the co-treated group, indicating the synergistic effects of BAY11-7082 and UCB-Exos (Figure 7(c)). In the context of inflammatory response, NF-κB signaling has been also known to be a key regulator of pro-inflammatory SASP components that contributed to delayed tissue regeneration by accumulating the senescent cells, dysregulating matrix remodeling, and chronic inflammation.[39–41] Therefore, we explored whether treatment with UCB-Exos, which suppresses NF-κB activation, could modulate SASP, particularly within the hair follicles. The results revealed that the mRNA expression of several inflammatory cytokines and ECM components associated with SASP were dramatically reduced after treatment with either UCB-Exos or BAY11-7082 (Figure 7(d)). These results suggested that the inhibition of NF-κB activation by UCB-Exos had the potential to mitigate the detrimental effects of SASP, thereby promoting a more favorable environment for tissue regeneration. Immunofluorescence staining demonstrated a prominent decrease in both NF-κB that was translocated into the nucleus and cytoplasmic IL-6 within the hair follicles after BAY11-7082 or UCB-Exos treatment (Figure 7(e)–(g)). Consequently, these hair follicles displayed reduced levels of apoptosis following BAY11-7082 or UCB-Exos treatment, with the lowest apoptotic rate observed after co-treatment (Figure 7(h) and (i)). Ultimately, NF-κB inhibition rescued the structural integrity of the hair follicles, including the DS, ORS, and hair bulbs, and protected the hair follicles against the transition to the degenerative catagen phase (Figure 7(j)). Taken together, our findings suggested that UCB-Exos effectively restored the hair follicles damaged by sUV through NF-κB inhibition.

Discussion

The skin serves as the body's primary defense against external threats, including chemical damage, physical injury, and microbial infection. This integumentary system comprises the epidermis, dermis, and skin appendages, and their interactions play a crucial role in maintaining skin homeostasis and promoting self-renewal during injury.[42] Advancing beyond the limitations of 2D-cultured cells, tissue-engineered skin grafts have been created as viable alternatives to natural skin.[43] These skin grafts have been fabricated by using 3D printing a range of biomaterials[44] or simply stacking keratinocytes and fibroblasts in a transwell to recapitulate layered dermal structures.[45] However, the engineered skin tissues have faced limitations due to their lack of skin appendages (hair follicles, sebaceous glands, neurons, and Merkel cells). This has led to the need for the development of sophisticated organoids with intricate tissue architecture.

Recently, Lee et al. first developed a three-dimensional hair-bearing SkOs derived from human iPSCs.[13] Unlike other technologies, based on skin developmental processes, iPSCs were self-organized into structures resembling the multi-layered skin tissue architectures, such as the epidermis, dermis, and various skin appendages including hair follicles. So far, several progresses have been made to optimize the culture conditions for iPSC-derived SkOs since SkOs were generated in the form of inside-out cysts with hyaline cartilages which might be physiologically irrelevant.[46,47] According to our previous work,[14] Wnt signaling activation enabled us to obtain large and pure SkOs without off-target cartilages. Moreover, to reflect the characteristics of the outermost layer of skin in direct contact with air, an air-liquid interface culture was employed after cutting the SkOs into sheet-like pieces, effectively inducing keratinization of skin surfaces as well as epidermal differentiation.[14,48] This system allowed us to obtain planar skin organoids with high structural maturity in which the epidermis, dermis, and hair follicles are stratified, akin to real skin. These SkOs can be usefully employed for studying the pathophysiology of skin diseases and drug efficacy testing.

It has been well established that exposure to UV radiation leads to significant structural damage in skin tissues.[49–51] The underlying pathological changes induced by UV radiation have been known to cause ECM breakdown, structural damage to keratin, DNA damage, and inflammation, which are dictated by various molecular pathways such as IκB-NF-κB signaling, generation of reactive oxygen species and cell cycle arrest.[52–54] In this study, we successfully developed an in vitro model of sUV-induced photodamage using SkOs, allowing us to closely replicate sUV-induced damage, such as skin barrier disruption, photo-burn, collagen fiber degradation, and pigmentation shown as an increase of melanocytes. Although the effects of UV radiation on skin have been extensively examined

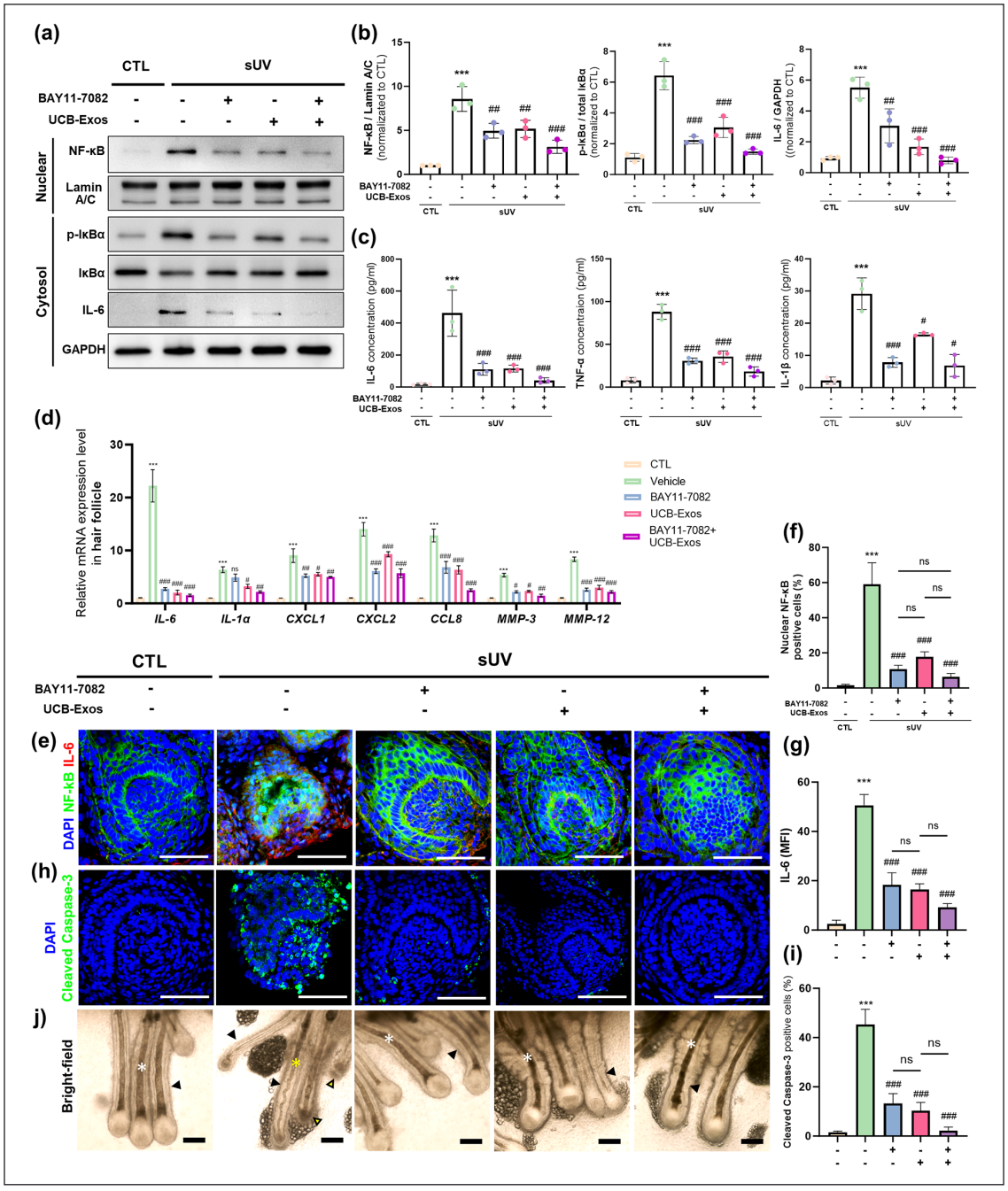

Figure 7. NF-κB inhibition effectively restored the hair follicles damaged by sUV exposur: (a) Western blot analysis of SkOs without sUV exposure and sUV-exposed SkOs that were treated with NF-κB inhibitor BAY11-7082 or UCB-Exos or both. The expression of NF-κB in the nuclear fraction and the expression of p- IκBα, total IκBα, and IL-6 in cytosol fraction in each group were analyzed, (b) quantification of nuclear NF-κB normalized to Lamin A/C, cytosol p-IκBα normalized to total IκBα, and cytosol IL-6 normalized to GAPDH ($n = 3$), (c) quantification of released proinflammatory cytokines, IL-6, TNF-α, and IL-1β from each group ($n = 3$), (d) qRT-PCR analysis of genes related to SASP in the hair follicles from each group ($n = 3$), (e) representative confocal images of each group stained with NF-κB (green), IL-6 (red), and DAPI (blue). Scale bar; 50 μm, (f), (g) quantification of the ratio of cells with NF-κB nuclear translocation (f) and MFI of IL-6 (g) in the stained sections of each group ($n = 3$). (h), (i) representative confocal images (h) and MFI quantification (i) of hair follicles stained with Cleaved Caspase-3 (green) and DAPI (blue) in each group. Scale bar, 50 μm ($n = 3$), (j) bright-field images of hair follicles in each group; healthy hair shaft (white asterisk), hair shaft in catagen phase (yellow asterisk) and ORS (black arrowhead). Note that NF-κB inhibition rescued the follicular structures and hair shafts in the sUV-damaged SkOs. Scale bar, 100 μm. Quantitative data were presented as a mean ± SD. Statistical differences between the groups were determined by ordinary one-way ANOVA with post-hoc Tukey test (b, c, f, g and i) and two-way ANOVA with post-hoc Bonferroni's test (d) (***$p < 0.001$ versus CTL, #$p < 0.05$, ##$p < 0.01$, ###$p < 0.001$ versus sUV-exposed SkO, ns; not statistically significant).

in both animal models and human epidermal and dermal models,[55–59] the impact on skin appendages, particularly hair follicles, has received relatively limited attention. Although some researchers previously investigated the responses of primary hair follicles isolated from human skin tissues after direct sUV irradiation,[60] this approach might not be appropriate because sUV naturally penetrates through the epidermis, dermis, and eventually reaches the hair follicles. In this light, we used the SkOs anchoring the hair follicles in dermal layers to explore the effects of sUV exposure on the hair follicles.[37] The results revealed that sUV exposure led to a marked elevation in apoptosis and structural disruption, particularly in $KRT5^+$ keratinocytes and fibroblasts in the dermal papilla cells of hair follicles. As a transition into the catagen phase of the anagen hair follicles was promoted by sUV exposure, the hair shaft became defective shown as kinking and thinning, indicating the deleterious effects of sUV on hair follicles. Indeed, it is noteworthy that increased hair loss has been reported in patients with repeated sUV exposure to the scalp skin.[61] Furthermore, we demonstrated a significant upregulation of pro-inflammatory cytokines within the hair follicles upon sUV irradiation, indicating inflammatory response closely linked to hair follicle damage.[62,63] These sUV-induced photodamaged hair follicles were further used to evaluate the efficacy of potential therapeutics.

Exosomes, composed of a rich array of biomolecules, proteins, nucleic acids, and metabolites, play a pivotal role in facilitating intercellular communication and influencing cellular immunity.[64] Due to their low immunogenicity and remarkable stability in body fluids, numerous studies have highlighted the therapeutic potential of cell-derived exosomes in the context of skin aging and hair follicle regeneration.[65,66] Of particular note are exosomes derived from MSCs, known for immunomodulatory and regenerative properties.[67] Hence, exosomes derived from MSCs show immense promise for a wide range of therapeutic applications.[16] In this context, sUV-exposed hair follicles in SkOs were treated with UCB-Exos as a therapeutic candidate. UCB-Exos effectively suppressed apoptosis, SASP, and pigmentation, while promoting the regeneration of hair follicles and repairing the follicular structures, suggesting the therapeutic efficacy of UCB-Exos in ameliorating UV-induced damage of hair follicles.

NF-κB signaling is known to play a central role in skin inflammation. It has even been shown that the mice with deleted genes activating the NF-κB pathway do not exhibit inflammatory changes, such as pro-inflammatory cytokine accumulation and edema, in skin tissues upon sUV exposure.[68] Considering that the UCB-derived exosomes have been known to mitigate inflammatory responses by inhibiting NF-κB activation,[69] we sought to elucidate the mechanism of actions of UCB-Exos, focusing on NF-κB mediated inflammatory responses. In our model, UV exposure increased the phosphorylation of IkBα and subsequent nuclear translocation of NF-κB in the hair follicles, leading to an increased secretion of pro-inflammatory cytokines. UCB-Exos effectively attenuated NF-κB activation and consequent inflammatory responses in the hair follicles. To further validate our findings, we compared UCB-Exos with BAY11-7082, a known NF-κB inhibitor. The effects of exosomes on repairing the hair follicular structures by inhibiting phosphorylated IkBα, NF-κB activation, and pro-inflammatory cytokine secretion were comparable to those of BAY11-7082. While the high-throughput transcriptomic analysis was not performed to identify the specific bioactive molecules contained in UCB-Exos that influences the NF-κB pathway, various assays provided the evidence that UCB-Exos implemented their therapeutic effects which structurally supported the hair follicle and protected the growing hair shaft through the NF-κB pathway in the sUV-exposed hair follicles. In particular, to analyze which of the cells composing the hair follicles are mainly affected, local expression of NF-κB and inflammatory cytokines was analyzed in the SkOs. Although various cells in the entire skin layers, including epidermal keratinocytes and dermal fibroblasts, are likely to be involved in skin inflammatory responses, we found that the interactions among hair-follicle residing cells, particularly keratinocytes in the ORS and matrix, were mainly responsible for NF-κB-mediated inflammatory response in sUV-exposed hair follicles. Additionally, NF-κB is generally recognized as an important factor in regulating cellular senescence and SASP through its role in inflammatory cascades.[70,71] We observed that both NF-κB inhibitor and UCB-Exos inhibited the SASP in the injured hair follicles of SkO, suggesting that UCB-Exos could manifest anti-aging functions beyond damage repair and anti-inflammation through the inactivation of NF-κB.

Meanwhile, there are some limitations to overcome in our study. First, there are possibilities that other inflammatory responses may be involved in sUV-induced hair follicle damage. For instance, it is known that when stimulated by UV irradiation, apoptosis, and ECM degradation may occur through the MAPK, TGF-β1, and NRF2 pathways, besides the NF-κB pathway.[66,67] Therefore, it needs to be further explored whether pathological changes of hair follicles in the SkOs and therapeutic mechanisms of UCB-Exos could be mediated by other pathways. In addition, inflammatory responses are mediated by both immune cells and non-immune cells, as the increased inflammatory cytokines due to sUV exposure may, in turn, stimulate immune cells. However, the lack of immune cells in SkOs remains a challenge. Thus, for a more accurate reflection of the pathophysiological responses occurring in the body, further investigation is needed to co-culture SkOs with various immune cells differentiated from iPSCs or modify the maturation protocols to induce the emergence of immune cells within the SkOs. Also, as the SkOs were exposed to sUV in a relatively mild and

short-term manner, further validation is required for severe or chronic exposure of sUV to hair follicles and the long-term effects of UCB-Exos on them. Moreover, the prolonged timelines required for SkO generation are particularly noted to pose significant challenges in achieving rapid outcomes in drug screening, especially in the fast-paced fields of pharmaceutical development and regenerative medicine. While SkOs require a complex and prolonged cultivation process to mimic the structures and functions of actual human skin, significant improvements to curtail SkO generation process are urgently needed to expand the clinical feasibility of SkOs. For instance, cryopreservation techniques for the immediate use of mature SkOs without compromising their integrity need to be explored to improve their utility.[72,73] However, the challenge still remains in creating personalized screening platforms with SkOs from patient-derived iPSCs in a timely manner. Hence, it is imperative to explore fundamental approaches to reducing the culture period of SkOs for efficient drug screening. One promising approach involves identifying and modulating key factors, such as Wnt/β-catenin, Sonic hedgehog, and BMP pathways, known to regulate the development of skin dermal layers as well as integral structures like hair follicles.[74–76] These interventions have the potential to considerably shorten the production timeline of SkOs, enhancing their utility as valuable drug screening platforms.

Despite these challenges, our photodamage model using SkOs is valuable for understanding the effects of UV exposure, particularly on the hair follicles, and elucidating the therapeutic mechanisms of UCB-Exos. The significant advantages of SkOs include their high structural complexity through self-assembly and the presence of skin appendages, enabling the reproduction of various skin lesions such as pathogen infection, dermatitis, alopecia, hyperpigmentation, and skin cancer. Thus, SkOs can serve as a useful platform for discovering therapeutic targets or drug screening for a variety of skin diseases. Moreover, this approach has the potential to be expanded into a platform for personalized medicine when using SkOs generated with patient-derived iPSCs.

Conclusions

In conclusion, SkOs derived from human iPSCs, representing the intricate structures of human skin, provide an innovative platform to study the effects of sUV exposure on the skin and, in particular, on hair follicles. Our SkOs subjected to sUV-induced damage exhibited the effects on follicular components, including disrupted structures and altered gene expression associated with hair growth. And this model allowed us to evaluate the therapeutic potential of UCB-Exos in sUV-induced hair follicle damage. Treatment of UCB-Exos effectively mitigated sUV-induced damage by suppressing inflammatory response through NF-κB inhibition and reducing SASP. Thus, this study established the utility of SkOs along with skin appendages as skin alternatives for studying skin biology and diseases. This approach also holds great promise as a valuable tool for high-throughput analysis and personalized drug screening.

Acknowledgements

Not applicable.

Author contributions

M.-J.K., D.-H.K., and K.-S.K. conceived and designed the study. M.-J.K. and H.-J.A. were involved in collection and/or assembly of data. M.-J.K., H.-J.A., and D.K. were involved in data analysis and interpretation. M.-J.K., D.-H.K., and K.-S.K. performed manuscript writing. S.L. and K.-S.K. were involved in administrative support. K.-S.K. did financial support. H.-J.A. and S.L were involved in the provision of study material. D.-H.K. and K.-S.K. did final approval of the manuscript. All authors read and approved the manuscript

Availability of data and materials

All datasets generated or analyzed during the current study are included in this published article and its Supplementary Information. Additional experimental details and more detailed data used or analyzed in this study are available from the corresponding author upon reasonable request.

Declaration of conflicting interests

The author(s) declared the following potential conflicts of interest with respect to the research, authorship, and/or publication of this article: The authors Min-Ji Kim, and Kyung-Sun Kang have a patent related to this paper (The patent application number is 1020230134662, Oct. 10, 2023).

Funding

The author(s) disclosed receipt of the following financial support for the research, authorship, and/or publication of this article: This work was supported by the Korean Fund for Regenerative Medicine (KFRM) grant (the Ministry of Science and ICT, the Ministry of Health & Welfare) No. 23A0101L1 funded by the Korea government.

Ethical approval statement

This study was carried out in accordance with the approved guidelines of the Seoul National University Institutional Review Board (Development of a disease model platform using stem cell-derived skin organoid-based technology, IRB No. 2211/003-013). The approved date was May 17th, 2023.

Consent for publication

Not applicable.

ORCID iD

Kyung-Sun Kang https://orcid.org/0000-0002-9322-741X

Supplemental material

Supplemental material for this article is available online.

References

1. Armstrong BK and Kricker A. The epidemiology of UV induced skin cancer. *J Photochem Photobiol B Biol* 2001; 63: 8–18.
2. Nogueira A, Joekes I and Dicelio L. About photodamage of human hair. *Photochem Photobiol Sci* 2006; 5: 165–169.
3. Zhai X, Gong M, Peng Y, et al. Effects of UV induced-photoaging on the hair follicle cycle of C57BL6/J mice. *Clin Cosmet Investi Dermatol* 2021; 14: 527–539.
4. Merin K, Shaji M and Kameswaran R. A review on sun exposure and skin diseases. *Indian J Dermatol* 2022; 67: 625.
5. Bernerd F and Asselineau D. An organotypic model of skin to study photodamage and photoprotection in vitro. *J Am Acad Dermatol* 2008; 58: S155–S159.
6. Sutterby E, Thurgood P, Baratchi S, et al. Evaluation of in vitro human skin models for studying effects of external stressors and stimuli and developing treatment modalities. *View* 2022; 3: 20210012.
7. Zhang JY. Chapter 15-Animal models of skin disorders. In: Conn PM (ed) Animal Models for the Study of Human Disease (Second Edition). Academic Press, 2017, pp.357–375.
8. Avci P, Sadasivam M, Gupta A, et al. Animal models of skin disease for drug discovery. *Expert Opin Drug Discov* 2013; 8: 331–355.
9. Danilenko DM, Phillips GDL and Diaz D. In vitro skin models and their predictability in defining normal and disease biology, pharmacology, and toxicity. *Toxicol Pathol* 2016; 44: 555–563.
10. Wufuer M, Lee G, Hur W, et al. Skin-on-a-chip model simulating inflammation, edema and drug-based treatment. *Sci Rep* 2016; 6: 37471.
11. Yan W-C, Davoodi P, Vijayavenkataraman S, et al. 3D bioprinting of skin tissue: from pre-processing to final product evaluation. *Adv Drug Deliv Rev* 2018; 132: 270–295.
12. Weng T, Wu P, Zhang W, et al. Regeneration of skin appendages and nerves: current status and further challenges. *J Transl Med* 2020; 18: 1–17.
13. Lee J, Rabbani CC, Gao H, et al. Hair-bearing human skin generated entirely from pluripotent stem cells. *Nature* 2020; 582: 399–404.
14. Jung S-y, You HJ, Kim M-J, et al. Wnt-activating human skin organoid model of atopic dermatitis induced by Staphylococcus aureus and its protective effects by Cutibacterium acnes. *Iscience* 2022; 25: 105150.
15. Kalluri RL and Valerie S. The biology, function, and biomedical applications of exosomes. *Science* 2020; 367: eaau6977.
16. Janockova J, Slovinska L, Harvanova D, et al. New therapeutic approaches of mesenchymal stem cells-derived exosomes. *J Biomed Sci* 2021; 28: 1–26.
17. Li M, Li S, Du C, et al. Exosomes from different cells: Characteristics, modifications, and therapeutic applications. *Eur J Med Chem*. 2020; 207: 112784.
18. Cho BS, Kim JO, Ha DH, et al. Exosomes derived from human adipose tissue-derived mesenchymal stem cells alleviate atopic dermatitis. *Stem Cell Res Ther* 2018; 9: 1–5.
19. Shin K-O, Ha DH, Kim JO, et al. Exosomes from human adipose tissue-derived mesenchymal stem cells promote epidermal barrier repair by inducing de novo synthesis of ceramides in atopic dermatitis. *Cells* 2020; 9: 680.
20. Zhang B, Wang M, Gong A, et al. HucMSC-exosome mediated-Wnt4 signaling is required for cutaneous wound healing. *Stem cells* 2015; 33: 2158–2168.
21. Rani S and Ritter T. The exosome – A naturally secreted nanoparticle and its application to wound healing. *Adv Mater* 2016; 28: 5542–5552.
22. Kim Y-J, Mi Yoo S, Park HH, et al. Exosomes derived from human umbilical cord blood mesenchymal stem cells stimulates rejuvenation of human skin. *Biochem Biophys Res Commun* 2017; 493: 1102–1108.
23. Liang J-X, Liao X, Li S-H, et al. Antiaging properties of exosomes from adipose-derived mesenchymal stem cells in photoaged rat skin. *BioMed Res Int* 2020; 2020: 6406395.
24. Kim JE, Heo YS and Lee KW. Osajin inhibits solar UV-induced cyclooxygenase-2 expression through direct inhibition of RSK2. *J Cell Biochem* 2017; 118: 4080–4087.
25. Biniek K, Levi K and Dauskardt RH. Solar UV radiation reduces the barrier function of human skin. *Proc Natl Acad Sci USA* 2012; 109: 17111–17116.
26. Pittayapruek P, Meephansan J, Prapapan O, et al. Role of Matrix Metalloproteinases in Photoaging and Photocarcinogenesis. *Int J Mol Sci* 2016; 17: 868.
27. Lee SJ, Lee KB, Son YH, et al. Transglutaminase 2 mediates UV-induced skin inflammation by enhancing inflammatory cytokine production. *Cell Death Dis* 2017; 8: e3148.
28. Zhang YL, Yan JJ, Li ZJ, et al. Exosomes derived from human umbilical cord mesenchymal stem cells alleviate psoriasis-like skin inflammation. *J Interf Cytok Res* 2022; 42: 8–18.
29. Bahta AW, Farjo N, Farjo B, et al. Premature senescence of balding dermal papilla cells is associated with p16 expression. *J Invest Dermatol* 2008; 128: 1088–1094.
30. Wlaschek M, Maity P, Makrantonaki E, et al. Connective tissue and fibroblast senescence in skin aging. *J Invest Dermatol* 2021; 141: 985–992.
31. Tavana O, Benjamin CL, Puebla-Osorio N, et al. Absence of p53-dependent apoptosis leads to UV radiation hypersensitivity, enhanced immunosuppression and cellular senescence. *Cell Cycle* 2010; 9: 3328–3336.
32. Müller K and Meineke V. Radiation-induced alterations in cytokine production by skin cells. *Exp Hematol* 2007; 35: 96–104.
33. Yu H, Lin LB, Zhang ZQ, et al. Targeting NF-κB pathway for the therapy of diseases: mechanism and clinical study. *Signal Transduct Tar* 2020; 5: 209.
34. Piipponen M, Li DQ and Landén NX. The Immune functions of keratinocytes in skin wound healing. *Int J Mol Sci* 2020; 21: 8790.
35. Wang JN, Duan ZM, Chen X, et al. The immune function of dermal fibroblasts in skin defence against pathogens. *Exp Dermatol* 2023; 32: 1326–1333.
36. Bora NS, Mazumder B, Mandal S, et al. Amelioration of UV radiation-induced photoaging by a combinational sunscreen formulation via aversion of oxidative collagen degradation and promotion of TGF-β-Smad-mediated collagen production (Retraction of Vol 127, Pg 261, 2019). *Eur J Pharm Sci* 2022; 177: 106245.
37. Gherardini J, Wegner J, Chéret J, et al. Transepidermal UV radiation of scalp skin induces hair follicle damage that is alleviated by the topical treatment with caffeine. *Int J Cosmetic Sci* 2019; 41: 164–182.

38. Lee J, Rhee MH, Kim E, et al. BAY 11-7082 is a broad-spectrum inhibitor with anti-inflammatory activity against multiple targets. *Mediat Inflamm* 2012; 2012: 416036.
39. Haga M and Okada M. Systems approaches to investigate the role of NF-kappaB signaling in aging. *Biochem J* 2022; 479: 161–183.
40. Gruber F, Kremslehner C, Eckhart L, et al. Cell aging and cellular senescence in skin aging – Recent advances in fibroblast and keratinocyte biology. *Exp Gerontol* 2020; 130: 110780.
41. Kang C, Xu Q, Martin TD, et al. The DNA damage response induces inflammation and senescence by inhibiting autophagy of GATA4. *Science* 2015; 349: aaa5612.
42. Takeo M, Lee W and Ito M. Wound healing and skin regeneration. *Cold Spring Harb Perspect Med* 2015; 5: a023267.
43. Xu Y, Wu X, Zhang Y, et al. Engineered artificial skins: current construction strategies and applications. *Eng Regen* 2023; 4: 438–450.
44. Abaci HE, Coffman A, Doucet Y, et al. Tissue engineering of human hair follicles using a biomimetic developmental approach. *Nat Commun* 2018; 9: 5301.
45. Miyake T and Shimada M. 3D organoid culture using skin keratinocytes derived from human induced pluripotent stem cells. *Methods Mol Biol* 2022; 2454: 285–295.
46. Ma J, Liu J, Gao D, et al. Establishment of human pluripotent stem cell-derived skin organoids enabled pathophysiological model of SARS-CoV-2 infection. *Adv Sci* 2022; 9: e2104192.
47. Ma J, Li W, Cao R, et al. Application of an iPSC-derived organoid model for localized scleroderma therapy. *Adv Sci* 2022; 9: e2106075.
48. Lei M, Schumacher LJ, Lai YC, et al. Self-organization process in newborn skin organoid formation inspires strategy to restore hair regeneration of adult cells. *Proc Natl Acad Sci USA* 2017; 114: E7101–E7110.
49. Ittycheri A, Lipsky ZW, Hookway TA, et al. Ultraviolet light induces mechanical and structural changes in full thickness human skin. *J Mech Behav Biomed Mater* 2023; 143: 105880.
50. Salminen A, Kaarniranta K and Kauppinen A. Photoaging: UV radiation-induced inflammation and immunosuppression accelerate the aging process in the skin. *Inflamm Res* 2022; 71: 817–831.
51. Watson RE, Gibbs NK, Griffiths CE, et al. Damage to skin extracellular matrix induced by UV exposure. *Antioxid Redox Signal* 2014; 21: 1063–1077.
52. Laszlo CF and Wu S. Mechanism of UV-induced IkappaBalpha-independent activation of NF-kappaB. *Photochem Photobiol* 2008; 84: 1564–1568.
53. Pillai S, Oresajo C and Hayward J. Ultraviolet radiation and skin aging: roles of reactive oxygen species, inflammation and protease activation, and strategies for prevention of inflammation-induced matrix degradation – a review. *Int J Cosmet Sci* 2005; 27: 17–34.
54. Pavey S, Russell T and Gabrielli B. G2 phase cell cycle arrest in human skin following UV irradiation. *Oncogene* 2001; 20: 6103–6110.
55. Sharma MR, Werth B and Werth VP. Animal models of acute photodamage: comparisons of anatomic, cellular and molecular responses in C57BL/6J, SKH1 and Balb/c mice. *Photochem Photobiol* 2011; 87: 690–698.
56. Lin MF, Liu XR, Wang XE, et al. A comparative study of skin changes in different species of mice in chronic photoaging models. *Int J Mol Sci* 2023; 24: 10812.
57. Bacqueville D, Douki T, Duprat L, et al. A new hair follicle-derived human epidermal model for the evaluation of sunscreen genoprotection. *J Photochem Photobiol B* 2015; 151: 31–38.
58. Natarajan VT, Ganju P, Ramkumar A, et al. Multifaceted pathways protect human skin from UV radiation. *Nat Chem Biol* 2014; 10: 542–551.
59. Qin JZ, Chaturvedi V, Denning MF, et al. Regulation of apoptosis by p53 in UV-irradiated human epidermis, psoriatic plaques and senescent keratinocytes. *Oncogene* 2002; 21: 2991–3002.
60. Lu Z, Fischer TW, Hasse S, et al. Profiling the response of human hair follicles to ultraviolet radiation. *J Invest Dermatol* 2009; 129: 1790–1804.
61. Piérard-Franchimont C, Quatresooz P and Piérard GE. *Effect of UV radiation on scalp and hair growth*, In: Trüeb RM and Tobin DJ (eds) Aging Hair. Berlin, Heidelberg: Springer Berlin Heidelberg, 2010, pp.113–121 2010.
62. Xu JM, Weng ZP, Arumugam A, et al. Hair follicle disruption facilitates pathogenesis to UVB-induced cutaneous inflammation and basal cell carcinoma development in mice. *Am J Pathol* 2014; 184: 1529–1540.
63. Zhang B, Zhao Y, Cai ZM, et al. Early stage alopecia areata is associated with inflammation in the upper dermis and damage to the hair follicle infundibulum. *Australas J Dermatol* 2013; 54: 184–191.
64. Yang GH, Lee YB, Kang D, et al. Overcome the barriers of the skin: exosome therapy. *Biomater Res* 2021; 25: 22.
65. Han JX, Wu T, Jin J, et al. Exosome-like nanovesicles derived from Phellinus linteus inhibit Mical2 expression through cross-kingdom regulation and inhibit ultraviolet-induced skin aging. *J Nanobiotechnol* 2022; 20: 455.
66. Duan M, Zhang Y, Zhang H, et al. Epidermal stem cell-derived exosomes promote skin regeneration by downregulating transforming growth factor-beta1 in wound healing. *Stem Cell Res Ther* 2020; 11: 452.
67. Wang T, Jian Z, Baskys A, et al. MSC-derived exosomes protect against oxidative stress-induced skin injury via adaptive regulation of the NRF2 defense system. *Biomaterials* 2020; 257: 120264.
68. Abeyama K, Eng W, Jester JV, et al. A role for NF-kappaB-dependent gene transactivation in sunburn. *J Clin Invest* 2000; 105: 1751–1759.
69. Zhang R, Zhu Y, Li Y, et al. Human umbilical cord mesenchymal stem cell exosomes alleviate sepsis-associated acute kidney injury via regulating microRNA-146b expression. *Biotechnol Lett* 2020; 42: 669–679.
70. Songkiatisak P, Rahman SMT, Aqdas M, et al. NF-kappaB, a culprit of both inflamm-ageing and declining immunity? *Immun Ageing* 2022; 19: 20.

71. Yasuda S, Horinaka M, Iizumi Y, et al. Oridonin inhibits SASP by blocking p38 and NF-κB pathways in senescent cells. *Biochem Biophys Res Commun* 2022; 590: 55–62.
72. Boonekamp KE, Kretzschmar K, Wiener DJ, et al. Long-term expansion and differentiation of adult murine epidermal stem cells in 3D organoid cultures. *Proc Natl Acad Sci USA* 2019; 116: 14630–14638.
73. Prinelli A, Silva-Almeida C, Parks S, et al. In-plate cryopreservation of 2D and 3D cell models: Innovative tools for biomedical research and preclinical drug discovery. *SLAS Discov* 2021; 26: 32–43.
74. Gilliver SC, Ruckshanthi JP, Atkinson SJ, et al. Androgens influence expression of matrix proteins and proteolytic factors during cutaneous wound healing. *Lab Invest* 2007; 87: 871–881.
75. St-Jacques B, Dassule H, Karavanova I, et al. Sonic hedgehog signaling is essential for hair development. *Curr Biol* 1998; 8: 1058–1069.
76. Kulessa H, Turk G and Hogan BL. Inhibition of Bmp signaling affects growth and differentiation in the anagen hair follicle. *EMBO J* 2000; 19: 6664–6674.